Supplementary Information

Light-activated agonist-potentiator of $GABA_A$ receptors for reversible neuroinhibition in wildtype mice

Galyna Maleeva[1,2,+], Alba Nin-Hill[3,+,‡], Ulrike Wirth[4], Karin Rustler[4,§], Matteo Ranucci[5], Ekin Opar,[1,2,6] Carme Rovira[3,7], Piotr Bregestovski[8,#], Hanns Ulrich Zeilhofer[5,9], Burkhard König[4], Mercedes Alfonso-Prieto[10,*], Pau Gorostiza[1,2,7,*]

1. Institute for Bioengineering of Catalonia (IBEC), The Barcelona Institute for Science and Technology, Barcelona, 08028 Spain

2. Networking Biomedical Center in Bioengineering, Biomaterials, and Nanomedicine (CIBER-BBN), ISCIII, Barcelona, 08028 Spain

3. Departament de Química Inorgànica i Orgànica (Secció de Química Orgànica) & Institut de Química Teòrica i Computacional (IQTCUB), Universitat de Barcelona, Barcelona, 08020 Spain

4. Institute of Organic Chemistry, University of Regensburg, Regensburg, 93053 Germany

5. Institute of Pharmacology and Toxicology, University of Zurich, Zürich, 8057 Switzerland

6. Doctorate program of the University of Barcelona, Barcelona, 08020 Spain

7. Catalan Institution for Research and Advanced Studies (ICREA), Barcelona, 08010 Spain

8. Institut de Neurosciences des Systèmes, UMR INSERM 1106, Aix-Marseille Université, Marseille, 13005 France

9. Institute of Pharmaceutical Sciences, Swiss Federal Institute of Technology (ETH) Zürich, Zürich, 8093 Switzerland

10. Institute of Neuroscience and Medicine INM-9 Computational Biomedicine, Forschungszentrum Jülich GmbH, D-52428 Jülich, Germany

+ equivalent contribution

* corresponding authors. E-mail: m.alfonso-prieto@fz-juelich.de (M. A. P.), pau@icrea.cat (P. G.)

‡ current address: Toulouse Biotechnology Institute, TBI, Université de Toulouse, CNRS, INRAE, INSA, F-31077 Toulouse Cedex, France

§ current address: Iris Biotech GmbH, Marktredwitz, 95615 Germany

 # current address: Institute of Neuroscience, Kazan State Medical University, Kazan, 420012 Russia

TABLE OF CONTENTS

Experimental Procedures

1. Molecular modeling

Docking was performed with Autodock Vina[1] (version 1.1.2). The initial structures of abecarnil and azocarnil (*Z*- and *E*-isomers) were created employing Avogadro[2] (version 1.1.1) and were subsequently optimized using quantum mechanics. Such calculations were performed with the Gaussian09 (G09) program package[3], using density functional theory[4,5], with the B3LYP functional[6] and the 6–31++G(d,p) basis set. The receptor model was taken from the cryo-electron microscopy structure of human $GABA_AR$ $\alpha_1\beta_2\gamma_2$ subtype solved in complex with DMCM[7] (methyl 6,7-dimethoxy-4-ethyl-β-carboline-3-carboxylate) (PDB 8DD3). We focused our docking calculations on the benzodiazepine binding site, i.e. the binding site for the parent compound abecarnil and for other β-carbolines such as DMCM (Figure 1). The search space was defined to enclose all the residues around 4 Å of the DMCM molecule in the experimental $GABA_AR$ structure[7], resulting in a box with side dimensions of 18 x 16 x 20 Å. The ligands were allowed to change their geometry (by exploring all the possible ligand torsions) to optimize its fitting to the benzodiazepine site, while the receptor was kept fixed. The maximum energy difference between the best and worst binding modes and the exhaustiveness of the search algorithm were set to default values (3 and 8 kcal·mol^{-1}, respectively). Instead, the maximum number of modes was increased to 20 to enhance docking sampling. This protocol was repeated 10 times, starting with different random seeds, so that a maximum total number of 200 binding modes could be obtained. The ligand binding poses were clustered using the CPPTRAJ tool from AmberTools21[8], using the k-means clustering algorithm, using as distance metric the ligand RMSD, with a maximum number of 10 clusters, randomizing the initial set of points and reaching a maximum of 500 iterations. The centroid of the most populated cluster was taken as representative structure and analyzed using the Binana2.1 algorithm[9,10]. Default values were used to identify protein-ligand interactions, except for the hydrogen and halogen bond angle cutoff, which was set to 90 degrees. Validation of the docking protocol was done by redocking DMCM and diazepam in their respective cryo-EM structures in complex with the human $GABA_AR$ $\alpha_1\beta_2\gamma_2$ subtype (PDB IDs 8DD3[7] and 6X3X[11], respectively). The representative docking poses obtained are almost identical to the experimentally determined binding poses for both ligands (see Figure S6), confirming the reliability of the docking protocol used. All the molecular modeling images were generated with VMD[12].

2.Reagents and working techniques

Starting materials and commercial reagents were purchased from Acros, Alfa Aesar, Fisher, Fluka, Fluorochem, Merck, Sigma-Aldrich, TCI and VWR and were used without further purification. Solvents were used in p.a. quality or dried according to common procedures if necessary. All reactions with oxygen- or moisture-sensitive reagents were carried out in glassware which was dried before use by heating under vacuum. Dry nitrogen or argon were used as inert gas atmosphere.

3.Analytical techniques

Nuclear magnetic resonance spectroscopy (NMR)

All NMR spectra were measured at room temperature using a Bruker Avance 400 (400 MHz for ^{1}H and 101 MHz for ^{13}C) or a Bruker Avance 600 (600 MHz for ^{1}H and 151 MHz for ^{13}C) NMR spectrometer. All chemical shifts are reported in δ-scale as parts per million [ppm] (multiplicity, coupling constant J, number of protons) relative to the solvent residual peaks. Coupling constants J are given in Hertz [Hz]. Abbreviations used for signal multiplicity: ^{1}H-NMR: s = singlet, d = doublet, dd = doublet of doublets, ddd = doublet of doublets of doublets, dt = doublet of triplets, t = triplet, td= triplet of doublets, q = quartet, and m = multiplet.

Mass spectrometry (MS)

All mass spectra were recorded on an Agilent Q-TOF 6540 UHD, Finnigan MAT SSQ 710 A, Jeol AccuTOF GCX or ThermoQuest Finnigan TSQ 7000 spectrometer.

UV-Vis absorption spectroscopy

Absorption spectra were recorded on a UV/VIS Agilent Cary 50 spectrometer.

Thin layer chromatography (TLC)

Analytical thin layer chromatography (TLC) was performed on silica gel coated alumina plates (MN precoated TLC-sheets ALUGRAM® Xtra SIL G/UV254). Visualization was done by UV-light (254 nm or 366 nm) or staining with ninhydrin solution.

Column chromatography

Column chromatography was performed on a Biotage Isolera One automated flash purification system with UV/Vis detector.

Analytical RP-HPLC

Analytical RP-HPLC were measured on an Agilent 1220 Infinity LC System (column: P/No 00F-4251-B0, Phenomenex Luna® 3 µm C18(2) 100 Å, LC column 150x2.0 mm).

Preparative RP-HPLC

Purification by preparative HPLC was conducted on a preparative HPLC Agilent 1260 Infinity LC System (column: P/No 00G-4253-P0-AX, Phenomenex Luna® 10 µm C18(2) 100 Å, LC column 250x21.2 mm). The eluent systems were used as specified. After the purification process, solvents were removed by lyophilization.

4.Experimental Procedures

Compounds **2**, **4**, **6**, **8**, **9**, **12** and **17** were commercially available and purchased from Sigma-Aldrich.

2-Methoxyacetaldehyde (**3**)[13]

1,1,2-Trimethoxyethane (**2**) (6.4 g, 7 mL, 54 mmol, 1.0 eq.) and water (15 mL) were refluxed overnight under nitrogen atmosphere. The mixture was cooled to rt and was extracted with CH_2Cl_2. The combined organic layers were dried over $MgSO_4$ and the solvent was removed carefully. The product was used due to its volatility and instability without any further purification in the next step.

N-Isopropyl-2-methoxyethan-1-imine (**5**)[14]

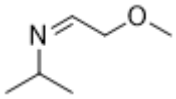

Isopropylamine (6.7 g, 9.3 mL, 113 mmol, 2.1 eq.) was dissolved in toluene (20 mL) in a nitrogen atmosphere. The mixture was cooled to 0 °C and **3** was added. After 30 min K_2CO_3 (5 g) was added. Subsequently, the mixture was filtered. The solution containing the product was used as such in the next step without any further purification.

N-(1-(1*H*-Indol-3-yl)-2-methoxyethyl)propan-2-amine (**7**)[14]

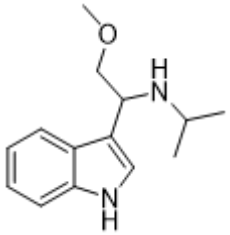

Indole (**6**) (3.7 g, 31 mmol, 1.0 eq.) was suspended in toluene (20 mL), acetic acid (20 mL), formic acid (14 mL) and isopropyl amine (7.0 mL). The mixture was cooled to -10 °C and a solution of imine **5** (1.6 eq.) was added slowly. The mixture was stirred for 1 h at rt. Water (60 mL) was added and the pH was adjusted to 12. The aqueous phase was extracted with toluene. The combined organic phases were

dried over $MgSO_4$ and the solvent was removed *in vacuo*. The crude product was purified by column chromatography (CH_2Cl_2/MeOH, 0-10%). **7** was obtained as an orange oil (4.2 g, 18 mmol, over three steps 33%).
^{1}H NMR (400 MHz, Chloroform-*d*) δ 10.16 (s, 1H), 9.62 (s, 1H), 7.86 (d, *J* = 2.7 Hz, 1H), 7.57 (d, *J* = 7.8 Hz, 1H), 7.47 – 7.43 (m, 1H), 7.25 – 7.16 (m, 2H), 4.79 (s, 1H), 4.00 (t, *J* = 9.8 Hz, 1H), 3.74 (dd, *J* = 10.2, 4.1 Hz, 1H), 3.42 (s, 3H), 3.25 (d, *J* = 9.2 Hz, 1H), 1.35 (dd, *J* = 8.2, 6.5 Hz, 6H).
^{13}C NMR (101 MHz, $CDCl_3$) δ 135.9, 126.6, 125.8, 123.1, 120.9, 117.2, 112.3, 105.6, 72.7, 59.1, 52.8, 48.4, 20.5, 19.0.
ESI-MS: m/z (%) = 233.17 $(M+H)^+$.

Ethyl (*E*)-2-((4-methoxybenzylidene)amino)acetate (**10**)[14]

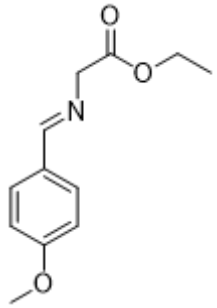

Glycine ethyl ester hydrochloride (**9**) (2.6 g, 25 mmol, 1.0 eq.) was dissolved in toluene (20 mL). 4-Methoxybenzaldehyde (**8**) (3.4 g, 3.0 mL, 25 mmol, 1.0 eq.) was added at rt. At 20 °C, triethylamine (2.8 g, 3.8 mL, 28 mmol, 1.1 eq.) was added dropwise and the resulting mixture was stirred at rt overnight. Then, water was added and the mixture was stirred for 15 min. The organic layer was separated, and the solvent was removed *in vacuo*. The crude product contained starting material and product but was used without further purification because the product decomposed during column chromatography. Yield: 66% (NMR analysis).
^{1}H NMR (400 MHz, Chloroform-*d*) δ 8.21 (d, *J* = 1.3 Hz, 1H), 7.75 – 7.68 (m, 2H), 6.95 – 6.89 (m, 2H), 4.35 (d, *J* = 1.2 Hz, 2H), 4.23 (q, *J* = 7.1 Hz, 2H), 3.83 (s, 3H), 1.29 (t, *J* = 7.1 Hz, 3H).
^{13}C NMR (101 MHz, $CDCl_3$) δ 170.5, 164.8, 162.2, 130.3, 128.7, 114.1, 62.2, 61.1, 55.5, 14.3.
EI-MS: m/z (%) = 221.10.
Ethyl 4-(methoxymethyl)-9*H*-pyrido[3,4-*b*]indole-3-carboxylate (**14**)[15]

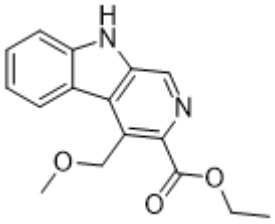

Compound **10** (3.88 g, 17.5 mmol, 1.0 eq.) was dissolved in DMF (15 mL) and K_2CO_3 (6.0 g) was added. The mixture was stirred at 98 °C. A solution of **7** (4.1 g, 17.5 mmol, 1.0 eq.) in DMF (25 mL) was added dropwise over 1 h. The reaction mixture was stirred at 98 °C for further 1.5 h. After cooling to rt and standing overnight, the formed precipitated was filtered off and washed with DMF. To the filtrate water (15 mL) and conc. HCl (2.5 mL) were added and the mixture was stirred for 20 min. In a separate flask, paraformaldehyde (568 mg, 18.9 mmol, 1.1 eq.) was suspended in water (15 mL) and conc. HCl (0.3 mL) and heated to 80 °C for 30 min until the solution became clear. The formaldehyde solution was cooled to rt and was added to the reaction mixture over 30 min. Stirring was continued at rt overnight. Water (65 mL) and toluene (50 mL) were added and the solution was stirred for 10 min. The organic phase was separated and sodium bicarbonate was added to the aqueous phase until a pH of 8 was reached. The water layer was extracted with toluene and the organic phases were combined, washed with water and dried over $MgSO_4$. The volume was reduced to 45 mL.

Then, the mixture was cooled to -15 °C and triethylamine (4.3 mL) was added in a nitrogen atmosphere. Under stirring, trichloroisocyanuric acid (2.44 g, 10.5 mmol) dissolved in ethyl acetate (60 mL) was added over 25 min, keeping the temperate below -8 °C. The mixture was stirred another 10 min at -10 °C and more triethylamine (5.1 mL) was added. The solution was stirred at rt overnight. Water was added (40 mL) and stirring was continued for 30 min. The organic phase was separated and the water phase was extracted with toluene. The organic phases were combined, washed with water and dried over $MgSO_4$. The solvent was removed *in vacuo* and the crude product was purified by column chromatography (PE/EtOAc, 50-100% and CH_2Cl_2/MeOH, 0-2%). Compound **14** was obtained as an off-white solid (516 mg, 1.8 mmol, 10% over three steps).

^{1}H NMR (400 MHz, Chloroform-*d*) δ 13.69 (s, 1H), 9.59 (s, 1H), 8.37 (dd, *J* = 8.3, 1.1 Hz, 1H), 7.82 (dt, *J* = 8.5, 1.0 Hz, 1H), 7.76 (ddd, *J* = 8.4, 6.9, 1.1 Hz, 1H), 7.47 (ddd, *J* = 8.2, 6.9, 1.1 Hz, 1H), 5.51 (s, 2H), 4.59 (q, *J* = 7.2 Hz, 2H), 3.52 (s, 3H), 1.54 (t, *J* = 7.1 Hz, 3H).

^{13}C NMR (101 MHz, $CDCl_3$) δ 160.9, 144.7, 136.3, 133.2, 132.5, 132.1, 128.1, 127.1, 125.8, 122.8, 120.5, 114.0, 66.2, 63.9, 58.7, 14.0.

ESI-MS: m/z (%) = 285.13 $(M+H)^+$.

Ethyl 4-(methoxymethyl)-6-nitro-9*H*-pyrido[3,4-*b*]indole-3-carboxylate (**15**)[16]

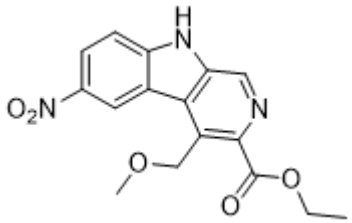

At 0 °C, concentrated nitric acid (14 mL) and fumic nitric acid (7 mL) were mixed carefully. Compound **14** (450 mg, 1.6 mmol, 1.0 eq.) was added portionwise. The reaction mixture was stirred for further 3 h at 5 °C. The solution was poured into ice water and neutralized with conc. ammonia solution. The precipitate was filtered, washed with water and dried to afford **15** as an off-white solid (473 mg, 1.4 mmol, 90%).

^{1}H NMR (400 MHz, DMSO-d_6) δ 12.75 (s, 1H), 9.12 (d, *J* = 2.3 Hz, 1H), 9.02 (s, 1H), 8.46 (dd, *J* = 9.1, 2.3 Hz, 1H), 7.83 (d, *J* = 9.1 Hz, 1H), 5.20 (s, 2H), 4.40 (q, *J* = 7.1 Hz, 2H), 3.39 (s, 3H), 1.37 (t, *J* = 7.1 Hz, 3H).

^{13}C NMR (101 MHz, DMSO) δ 166.7, 144.3, 140.9, 139.7, 138.0, 134.4, 127.5, 127.2, 123.5, 121.8, 120.0, 112.8, 67.4, 61.2, 57.6, 14.2.

ESI-MS: m/z (%) = 330.11 $(M+H)^+$.

Ethyl 6-amino-4-(methoxymethyl)-9*H*-pyrido[3,4-*b*]indole-3-carboxylate (**16**)[16]

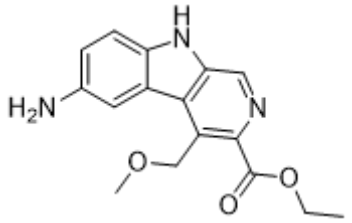

Compound **15** (433 mg, 1.3 mmol, 1.0 eq.) was dissolved in methanol (50 mL). Pd/C (10%, 130 mg) was added and the reaction mixture was stirred under hydrogen (1 bar) for 3 h at rt (TLC monitoring and staining with ninhydrin). The mixture was filtered over celite and the solvent was removed *in vacuo*. Amine **16** was used without further purification in the next step.

^{1}H NMR (400 MHz, DMSO-d_6) δ 12.28 (s, 1H), 8.96 (s, 1H), 8.18 (d, *J* = 2.1 Hz, 1H), 7.78 (d, *J* = 8.7 Hz, 1H), 7.54 (dd, *J* = 8.7, 2.1 Hz, 1H), 5.16 (s, 2H), 4.39 (q, *J* = 7.1 Hz, 2H), 3.38 (s, 3H), 1.36 (t, *J* = 7.1 Hz, 3H).

ESI-MS: m/z (%) = 300.13 $(M+H)^+$.

Ethyl (*E*)-4-(methoxymethyl)-6-(phenyldiazenyl)-9*H*-pyrido[3,4-*b*]indole-3-carboxylate (**1**)[17]

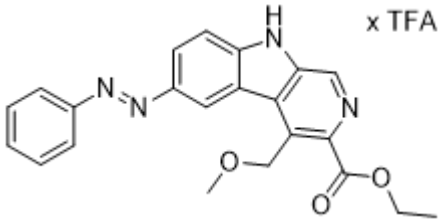

Compound **16** (363 mg, 1.21 mmol, 1.0 eq.) and nitrosobenzene (**17**) (130 mg, 1.21 mmol, 1.0 eq.) were stirred in AcOH (70 mL) and CH_2Cl_2 (10 mL) overnight at 40 °C. The solvent was removed *in vacuo*. Purification by preparative HPLC (column: Phenomenex Luna 10 µm C18(2) 100 Å, gradient 0-20 min: MeCN/0.05% aqueous TFA 10:90 – 98:2), evaporation, and lyophilization of the solvent yielded **1** (351 mg, 0.70 mmol, 58%) as a yellow solid.

^{1}H NMR (400 MHz, DMSO-d_6) δ 12.47 (s, 1H), 8.97 (s, 1H), 8.83 (d, *J* = 1.9 Hz, 1H), 8.21 (dd, *J* = 8.9, 1.9 Hz, 1H), 7.98 – 7.90 (m, 2H), 7.82 (d, *J* = 8.9 Hz, 1H), 7.66 – 7.58 (m, 2H), 7.57 – 7.50 (m, 1H), 5.25 (s, 2H), 4.40 (q, *J* = 7.1 Hz, 2H), 3.42 (s, 3H), 1.37 (t, *J* = 7.1 Hz, 3H).

^{13}C NMR (101 MHz, DMSO) δ 166.9, 152.0, 146.1, 143.0, 139.3, 137.5, 133.9, 130.8, 129.4, 127.8, 127.1, 123.1, 122.3, 121.1, 120.8, 113.1, 67.5, 61.0, 57.6, 14.2.

HR-MS (ESI): calc. for $C_{22}H_{20}N_4O_3$ $(M+H)^+$, m/z 389.1608, found: 389.1613.

Purity

Purity was measured in DMSO at the detection wavelenghts 220 nm and 254 nm.

Purity (220 nm): 100%, Purity (254 nm): 99%

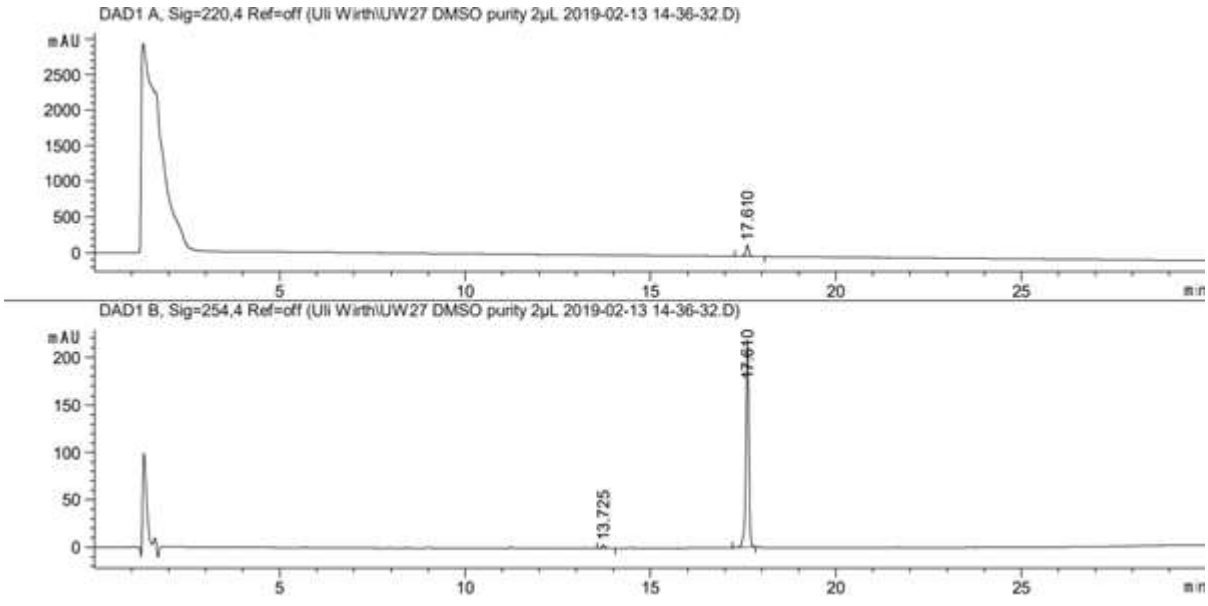

Signal 1: DAD1 A, Sig=220,4 Ref=off

Peak #	RetTime [min]	Type	Width [min]	Area [mAU*s]	Height [mAU]	Area %
1	17.610	BB	0.0841	912.38580	161.07248	100.0000
Totals :				912.38580	161.07248	

Signal 2: DAD1 B, Sig=254,4 Ref=off

Peak #	RetTime [min]	Type	Width [min]	Area [mAU*s]	Height [mAU]	Area %
1	13.725	BB	0.0774	16.79308	3.29575	1.3674
2	17.610	BB	0.0827	1211.32825	218.27760	98.6326
Totals :				1228.12132	221.57335	

Figure S1. Purity of Azocarnil (**1**) determined at 220 nm and 254 nm by RP-HPLC.

5. Photostationary State

Photostationary states (PSS) were measured on analytical HPLC (flow: 0.3 mL/min, solvent A: H_2O (0.05 % TFA), solvent B: MeCN). To determine the photostationary state of the photoswitch the samples (0.1 mM in DMSO) were irradiated first with 400 nm to get the *Z*-isomer. Afterwards, the sample was irradiated with 505 nm, to get back to the *E*-isomer. The samples were measured at the isosbestic point (439 nm). The aqueous buffer used for the determination of the photostationary state in the aqueous solution: 25 mM HEPES, 2.5 mM $CaCl_2$, 1 mM $MgCl_2$, pH = 7.4.

***Z*-Isomer: 87%**

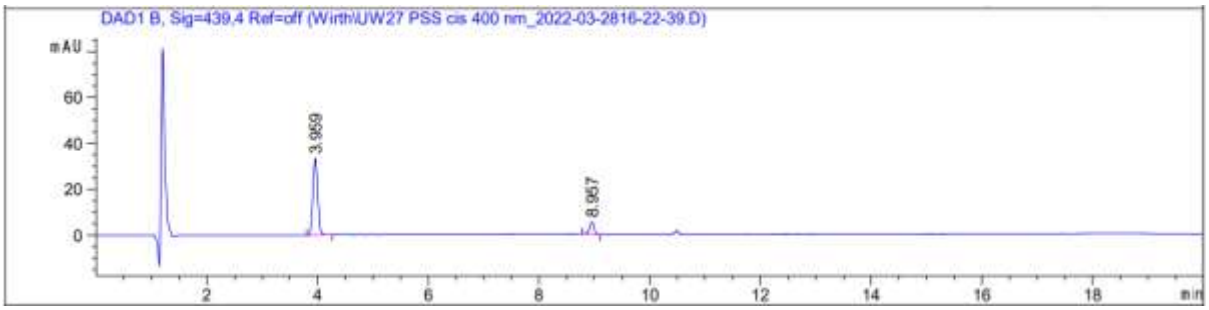

Signal 2: DAD1 B, Sig=439,4 Ref=off

Peak #	RetTime [min]	Type	Width [min]	Area [mAU*s]	Height [mAU]	Area %
1	3.959	BB	0.0939	199.69797	33.31297	86.8313
2	8.957	BB	0.0892	30.28584	5.25516	13.1687
Totals :				229.98380	38.56813	

***E*-Isomer: 75%**

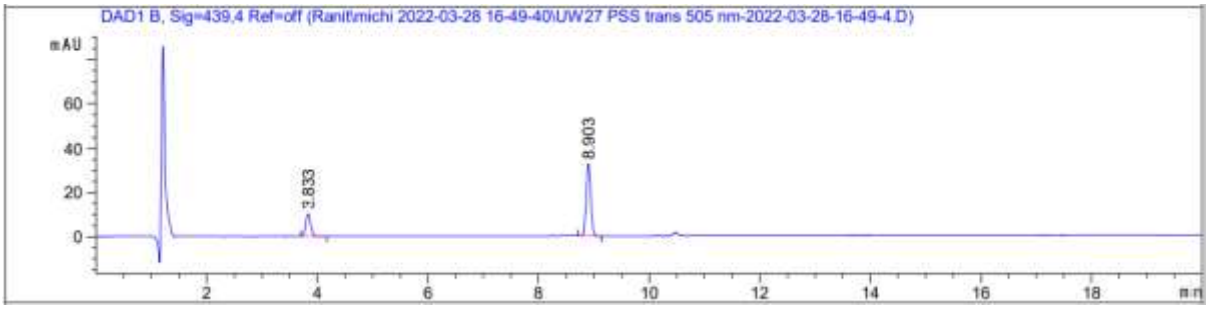

Signal 2: DAD1 B, Sig=439,4 Ref=off

Peak #	RetTime [min]	Type	Width [min]	Area [mAU*s]	Height [mAU]	Area %
1	3.833	BB	0.0981	62.29324	10.08276	24.9345
2	8.903	BB	0.0905	187.53395	32.90730	75.0655
Totals :				249.82719	42.99006	

Figure S2. Photostationary states of *Z*- and *E*-isomer after irradiation with 400 nm and 505 nm, respectively. Measured at the isosbestic point by RP-HPLC.

6. Primary culture of hippocampal neurons

Procedures were performed in accordance with the European guidelines for animal care and use in research (EU directive 2010/63/EU and Spanish guidelines, Laws 32/2007, 6/2013, and RD 53/2013) and were approved by the Animal Experimentation Ethics Committee of the Barcelona Science Park (PCB, 21-000-PG).
Sprague-Dawley rat pups (P 1-5) were sacrificed by decapitation, hippocampi were isolated and treated with 0.1 % trypsin in HBSS (10 min, 37ºC). Neurons were plated on Poly-D-Lysine (PDL)-coated 16 mm coverslips (0.5-1 x 105 cells) and incubated at 37^{o}C, 5% CO2 for 1.5 hours (to allow cells adhesion) in MEM supplemented with heat-inactivated FBS (5 %), heat-inactivated HS (5 %), penstrep (10 UI/ml), L-glutamine (2 mM) and glucose (20 mM). Cells were cultured in Neurobasal A medium, supplemented with B-27 (5 %), penstrep (5 UI/ml), glutaMAX (0.5x) and glucose (15 mM). On DIV 3 (third day in vitro) cultured cells were treated with 1 µM of Ara-C to prevent proliferation of non-neuronal cells. 50% of the maintenance medium was exchanged every 4 days. Electrophysiology experiments were performed on neurons older than 12 DIV.

7. Electrophysiological recordings and data analysis

Whole-cell recordings were performed at room temperature using an EPC-10 amplifier (HEKA Elektronik, Germany) and Patch Master software (HEKA). Cells were bathed with external solution containing (mM): 150 NaCl, 3 KCl, 2 $MgCl_2$, 10 HEPES, 10 D-glucose and 2 $CaCl_2$; pH was adjusted to 7.4 with NaOH. Recording pipettes were pulled from borosilicate glass capillaries (Harvard Apparatus Ltd, USA) and had resistance 5-10 MOhms. Solution used for filling patch contained (mM): 130 KCl, 10 HEPES, 1 $MgCl_2$, 3 Mg-ATP, 1 Na-GTP, 0.5 EGTA
Miniature GABAergic inhibitory postsynaptic currents (mIPSCs) were recorded in voltage clamp configuration in the presence of tetrodotoxin (TTX, 1µM) and CNQX (10 µM) and AP5 (40 µM) to block Nav channel, AMPA and NMDA receptors-mediated currents, respectively. To block mIPSCs, bicuculline (25 µM) was used, or picrotoxin (PTX, 100 µM); the former is a competitive antagonist of $GABA_A$ receptors, whereas the latter is a pore blocker of GABA and glycine receptors. Recordings were made at holding potential of -70 mV.
Azocarnil and PTX were first dissolved in DMSO and then in the bath solution till the final concentration. TTX, CNQX, AP5 and bicuculline were first dissolved in MilliQ water and then in the bath solution till the final concentration.
Photostimulation of azocarnil in patch-clamp experiments was done using a Till Photonics Polychrome V monochromatic light source with a 150 W xenon lamp and a slit selecting ± 10 nm spectral bands controlled by Patch Master software (HEKA). The light power measured with an Ophir light meter (Ophir Optronics Solutions) placed after the 20x objective was 0.34 $mW \cdot cm^{-2}$ for 400 nm, and 0.94 $mW \cdot cm^{-2}$ for 500 nm light.
Data were analyzed using Igor Pro 6.05 (WaveMatrics, USA) and Prism 9 (GraphPad, USA) software. Results are represented as mean ± SD. Statistical difference between groups was evaluated with paired and unpaired t-test and was considered significant at the value of P below 0.05.

8. Fiber optic cannula implantation

Six- to eight-week-old, C57BL/6 wild-type mice were implanted with cannulas for local light delivery as previously described[18]. In brief, mice were anesthetized with 5% isoflurane and kept under anesthesia with 2-3% isoflurane on a stereotaxic frame throughout the duration of the surgery. After shaving the fur on the back of each mouse, a skin incision was made to expose the vertebral column and cuts were performed on the muscles located medially to the longitudinal tendons running along the vertebral bodies, in order to better expose the vertebrae. The vertebral column was subsequently clamped at level of the thirteenth thoracic vertebra (T13). After carefully removing connective tissue

and absorbing excessive bleeding with collagen strips (Lyostypt, B. Braun), a hole was drilled approximately 1 mm left of the spinous process of the T13 vertebra. After placing the cannulas (Doric lenses) with ferrules (⌀ 1.25 mm) on the drilled hole, two layers of 3M™ Scotchbond™ Universal Self Etch Adhesive were applied and cured with UV light for 10 s each to fix the cannula in place. To ensure a more stable implant, Tetric Evoflow® A1 (Ivoclar vivadent) was subsequently applied and also cured with UV light for 10 s. The muscles along the vertebral column were then sutured using absorbable sutures (Safil 5-0, B. Braun). The skin was sutured with non-absorbable threads (Dafilon 6-0, B. Braun). Mice were allowed to recover on a heat pad. Behavioral experiments were conducted 7 days after surgery.

9. Behavioral experiments

To measure the effect of photoactivated azocarnil on mechanical sensitivity, mice were placed in plexiglass cylinders (10x10 cm wide, 25 cm high) on a grid, in order to have access to the plantar side of the hindpaws. Azocarnil (300 µM in 10 µl of ACSF, from 10 mM stock dissolved in DMSO) was injected intrathecally between vertebrae L5 and L6 under brief anesthesia with 2% isoflurane using a 10 µl Hamilton syringe and a 30-gauge needle. Immediately before the sensory testing, cannulas were connected to the optical fiber (0.39 NA multimode fiber-optic patch cable, Thorlabs, Inc) through a mating sleeve. The fiber was coupled to a UV LED module (PlexBright UV LED module, 405 nm, Plexon, Inc) and intensity was controlled through a current generator (Plexon, LED Driver LD-1, Plexon, Inc). An output current of 50 mA was sufficient to produce a light power ranging between 10 – 20 µW at the outlet of the implanted cannula. Light power was measured *ex vivo* after the end of the sensory testing, using a fiber optic power meter with internal sensor (Thorlabs, Inc). Light intensities above 50 mA triggered aversive behaviors (mainly back arching).
Mechanical sensitivity was tested using von Frey filament stimulation of the plantar side of the left hindpaw. Sensitivity was defined as the force that triggered withdrawal responses in 50% of the trials (using the Up-Down reader software described previously[19]). Mice were habituated on the test chamber for at least 1 hour before testing.
Motor coordination was assessed using the rotarod test (IITC, Woodland Hills, CA) with rotational speed accelerating from 4 to 40 rpm over 300 s. Two training sessions were performed before the latency to fall was measured in 5 test sessions per mouse. Permission for all animal experiments was obtained from the Kanton of Zurich (license 097/2021). All animal experiments complied with the relevant ethical regulations.

Supplementary figures

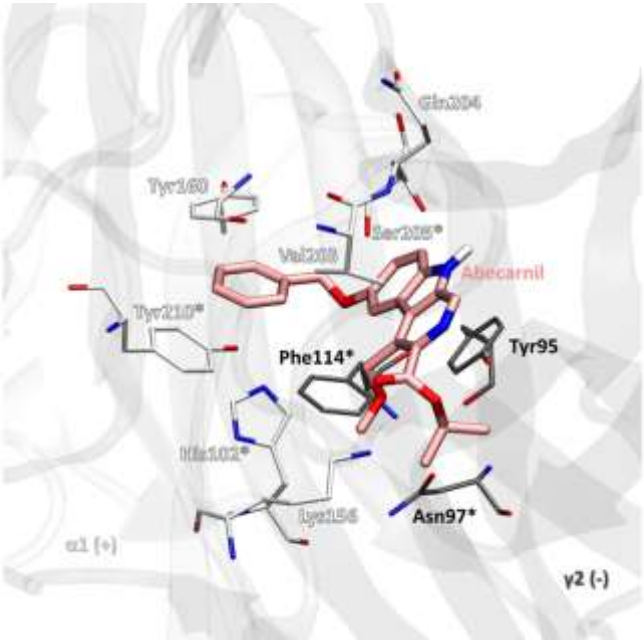

Figure S3. Representative docking poses for abecarnil bound in the benzodiazepine binding site of $GABA_AR$. Abecarnil (pink and thicker lines) and $GABA_AR$ interacting residues (thinner lines, in white for the principal (+) side of the α1 subunit and gray for the complementary (-) side of the γ2 subunit) are shown. The * symbol indicates the residues for which mutagenesis data is available demonstrating their importance for β-carboline and benzodiazepine binding to the benzodiazepine site (see Table S1).

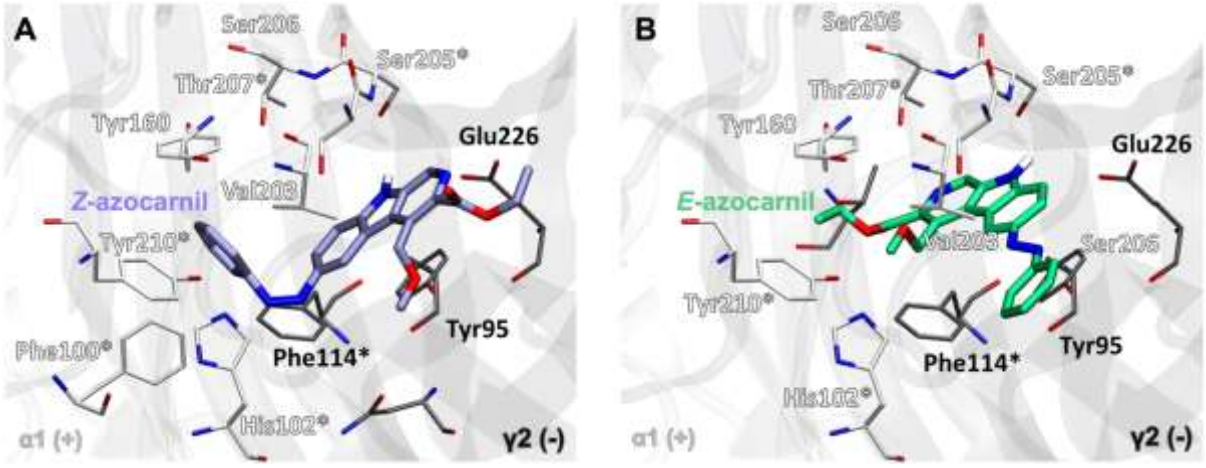

Figure S4. Representative docking poses for *Z* and *E* azocarnil bound in the benzodiazepine binding site of $GABA_AR$. (A) *Z*-azocarnil (violet and thicker lines) and $GABA_AR$ interacting residues (thinner lines, in white for the principal (+) side of the α1 subunit and gray for the complementary (-) side of γ2 subunit) are shown. **(B)** *E*-azocarnil (green and thicker lines) and $GABA_AR$ interacting residues (using the same representation as in panel A) are shown. The * symbol indicates the residues for which mutagenesis data is available demonstrating their importance for β-carboline and benzodiazepine binding to the benzodiazepine site (see Table S1).

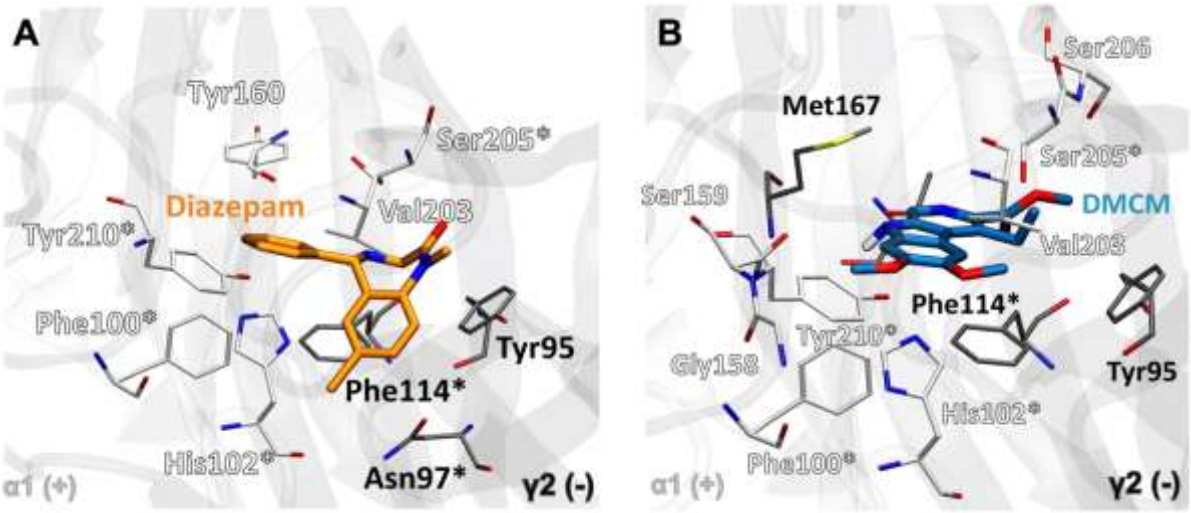

Figure S5. Crystallographic binding poses of diazepam and DMCM in the benzodiazepine binding site of GABA$_A$R. (A) Diazepam (orange and thicker lines) and the GABA$_A$R interacting residues (thinner lines in white for the principal (+) side of the α1 subunit and gray for the complementary (-) side of the γ2 subunit) are shown, based on PDB 6X3X[11]. **(B)** DMCM (steel blue and thicker lines) and GABA$_A$R interacting residues (same representation as in panel A) are shown, based on PDB 8DD3[7]. The * symbol indicates the residues for which mutagenesis data is available demonstrating their importance for β-carboline and benzodiazepine-like binding to the benzodiazepine site (see Table S1).

Table S1. GABA$_A$R residues involved in binding to the benzodiazepine site for each of the representative pose of the most populated cluster (population indicated in percentage) of the ligands discussed in the main text, classified based on the interaction type, as identified with Binana 2.1[9]. The * symbol indicates the residues for which mutagenesis data is available demonstrating their importance for β-carboline and benzodiazepine binding to the benzodiazepine site[7, 20–23, 24].

	Abecarnil (30%)	***Z*-Azocarnil** (22%)	***E*-Azocarnil** (28%)	**Diazepam**	**DMCM**
Hydrogen Bonds		α1 His102*			α1 His102*
	α1 Lys156				
	α1 Gln204				
	α1 Ser205*		α1 Ser205*	α1 Ser205*	
		α1 Ser206	α1 Ser206		α1 Ser206
			γ2 Thr179		γ2 Thr179
		γ2 Glu226	γ2 Glu226		
Hydrophobic		α1 Phe100*		α1 Phe100*	α1 Phe100*
	α1 His102*	α1 His102*		α1 His102*	α1 His102*
					α1 Gly158
					α1 Ser159
	α1 Tyr160	α1 Tyr160	α1 Tyr160	α1 Tyr160	α1 Tyr160
	α1 Val203	α1 Val203	α1 Val203	α1 Val203	α1 Val203
	α1 Ser205*	α1 Ser205*	α1 Ser205*	α1 Ser205*	α1 Ser205*
			α1 Thr207*		
	α1 Tyr210*	α1 Tyr210*	α1 Tyr210*	α1 Tyr210*	α1 Tyr210*
	γ2 Tyr95	γ2 Tyr95	γ2 Tyr95	γ2 Tyr95	γ2 Tyr95
	γ2 Asn97*				
	γ2 Phe114*	γ2 Phe114*	γ2 Phe114*	γ2 Phe114*	γ2 Phe114*
					γ2 Met167

		γ2 Glu226	γ2 Glu226		
π-π stacking		α1 Phe100*			
	α1 Tyr160			α1 Tyr160	α1 Tyr160
	α1 Tyr210*			α1 Tyr210*	α1 Tyr210*
	γ2 Tyr95	γ2 Tyr95	γ2 Tyr95		
				γ2 Phe114*	γ2 Phe114*
Halogen Bonds				α1 His102*	
				γ2 Asn97*	

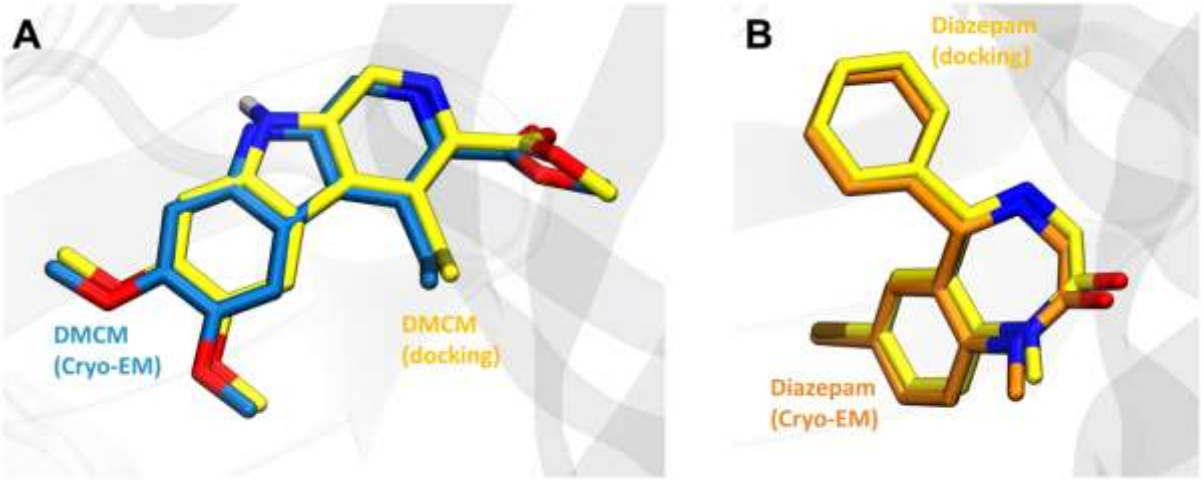

Figure S6. Superposition of the representative docking poses for DMCM and diazepam with their corresponding experimental poses bound in the benzodiazepine binding site of $\alpha_1\beta_2\gamma_2$ GABA$_A$R. (A) Representative docking pose of the most populated cluster (yellow) and cryo-EM pose blue, PDB ID 8DD3[7], for DMCM. **(B)** Representative docking pose of the most populated cluster (yellow) and the cryo-EM pose (orange, PDB ID 6X3X[11]) for diazepam.

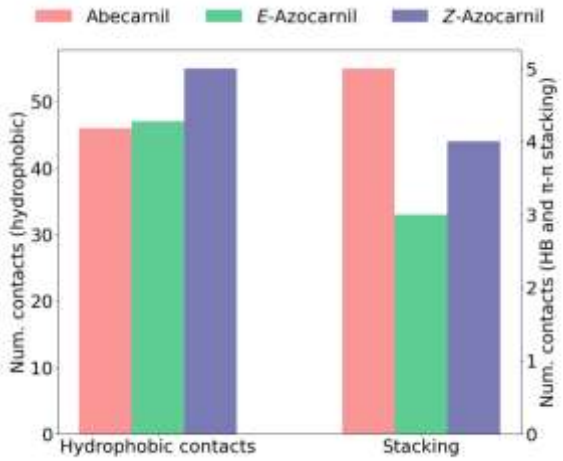

Figure S7. Molecular docking calculations of abecarnil, *E* and *Z*-Azocarnil in the benzodiazepine binding site of the GABA$_A$ receptor. Number of contacts (i.e. hydrophobic interactions, stacking interactions) for the representative docking poses of abecarnil (pink), *E*-azocarnil (green), and *Z*-azocarnil (violet) shown in Figure 2 in the main text.

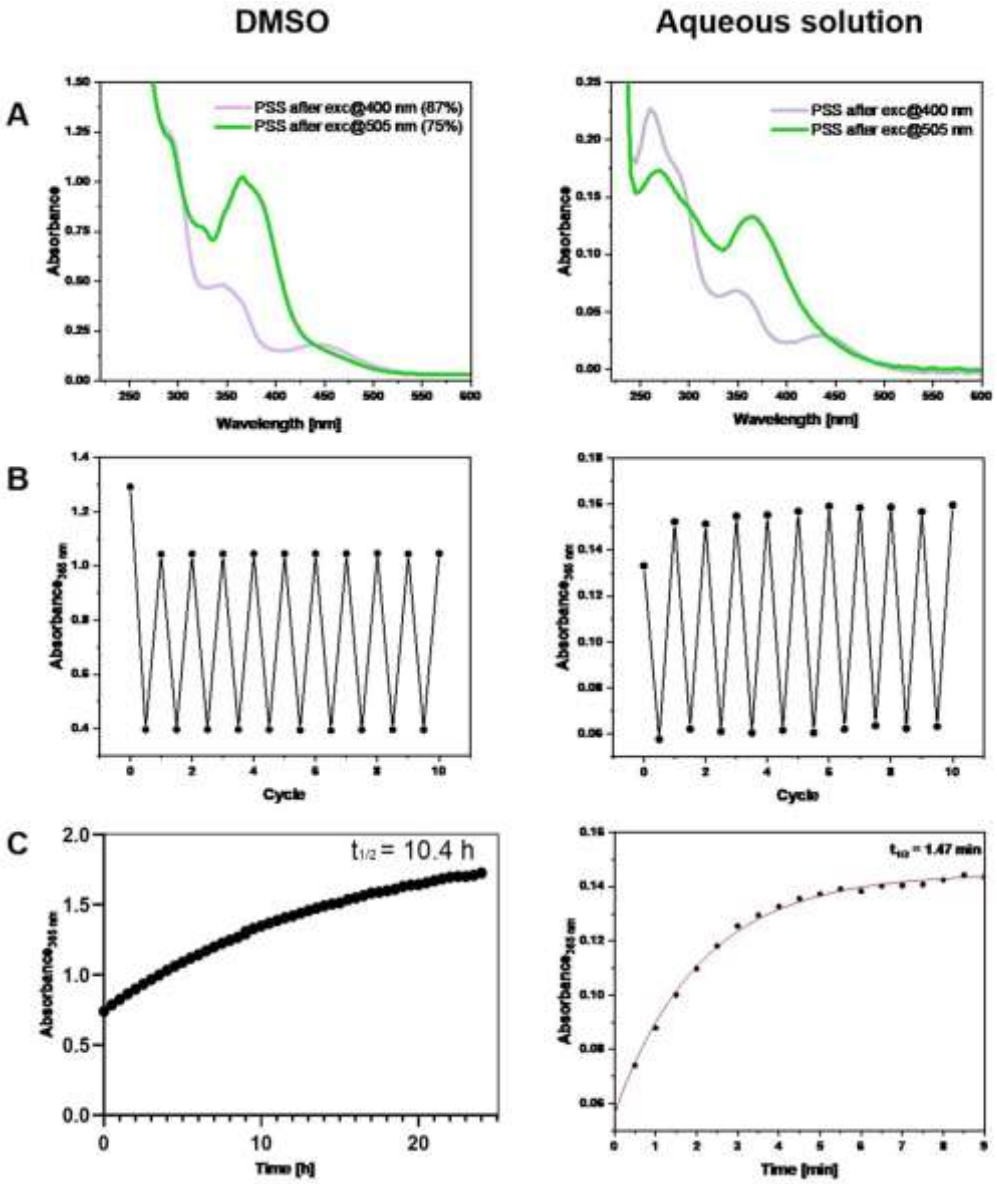

Figure S8. Photophysical properties of azocarnil in DMSO (50 µM, left) and in aqueous HEPES buffer (25 µM + 0.5 % DMSO, right). (A) UV-visible spectra of azocarnil after excitation at 400 nm (purple line, reaching a photostationary state (PSS) of 87 % Z isomer as determined by HPLC) and at 505 nm (green line, reaching a PSS of 75 % E isomer). These wavelengths were chosen to produce maximal photoconversion to Z and E isomers, respectively, considering the relative absorbance between the isomers instead of their maxima. **(B)** Cycle performance to evaluate photofatigue. **(C)** Thermal relaxation half-lives in the dark (black: measured data points, red: fitting line) are 10.4 h (lifetime 15.0 h, rate 0.07 h^{-1}) in DMSO and 1.5 min in aqueous buffer (lifetime 2.1 min, rate 0.47 min^{-1}). The compound was illuminated under 400 nm for 10 min at 0.84 $mW \cdot cm^{-2}$ and kept in the dark for relaxation measurements.

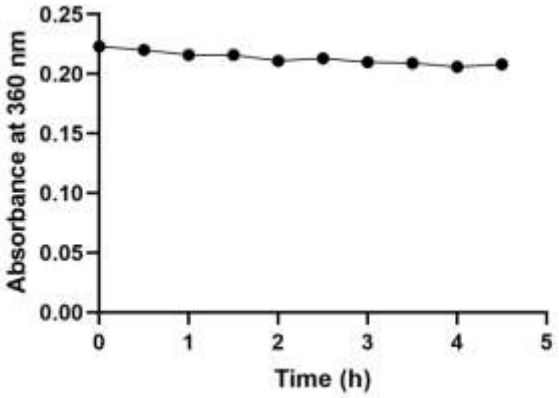

Figure S9. Stability of azocarnil in aqueous HEPES buffer (25 µM + 0.5 % DMSO). Although no signs of precipitation are observed in aqueous 25 µM azocarnil solution during several hours, the absorbance at 360 nm is reduced from 0.22 at time zero to 0.21 at 4.5 h, corresponding to 1 % decrease every hour. This result indicates sufficient stability to perform the biological experiments reported in Figures 3 and 4.

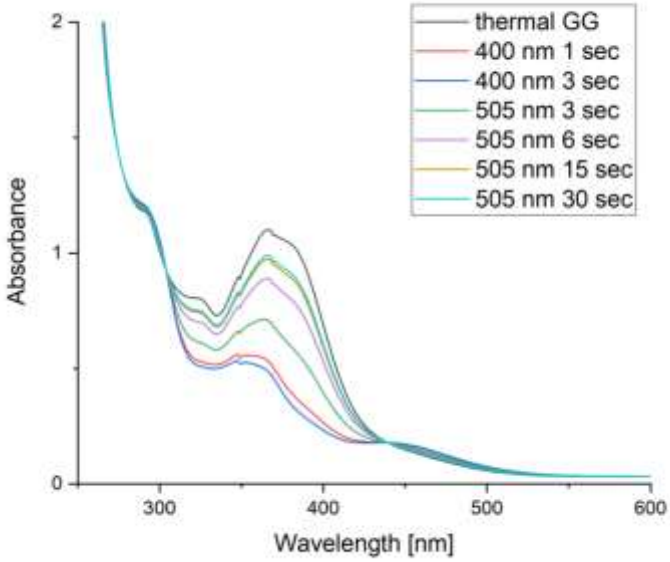

Figure S10. Absorption spectra of 50 µM azocarnil in DMSO at different time points under 400 nm and 505 nm illumination. E-Z photoconversion reaches a plateau in 3 s at 400 nm and Z-E photoconversion saturates in 30 s at 505 nm. The isosbestic points are 305 nm and 440 nm.

NMR Spectra

N-(1-(1*H*-Indol-3-yl)-2-methoxyethyl)propan-2-amine (**7**)

^{1}H-NMR

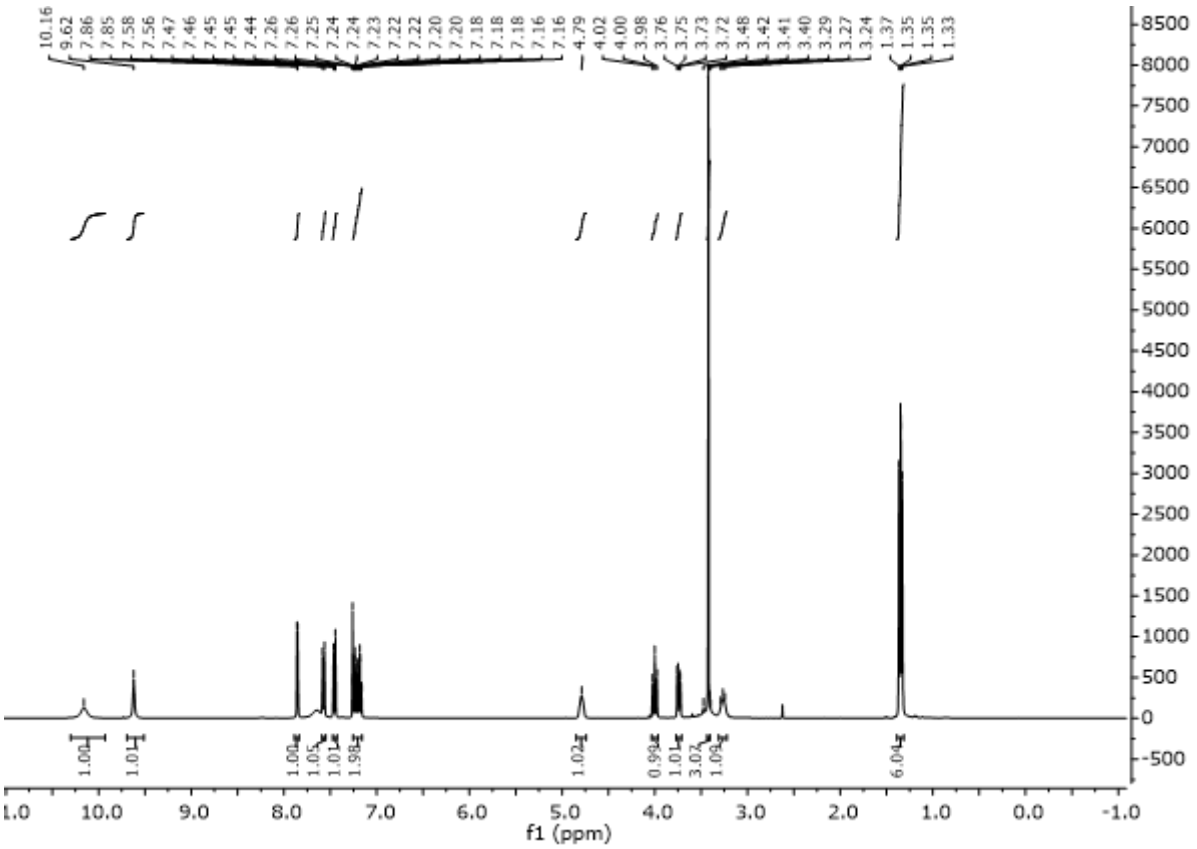

^{13}C-NMR

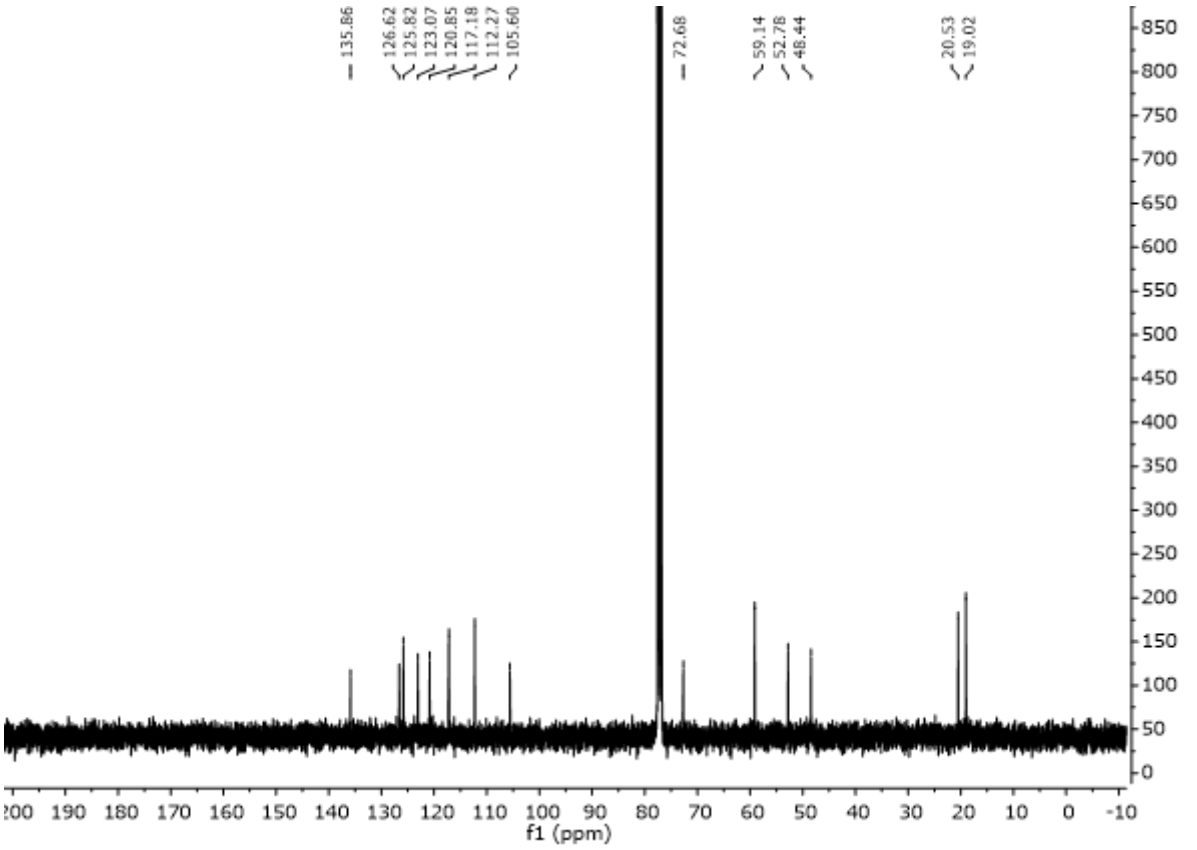

Ethyl (*E*)-2-((4-methoxybenzylidene)amino)acetate (**10**)

^{1}H-NMR

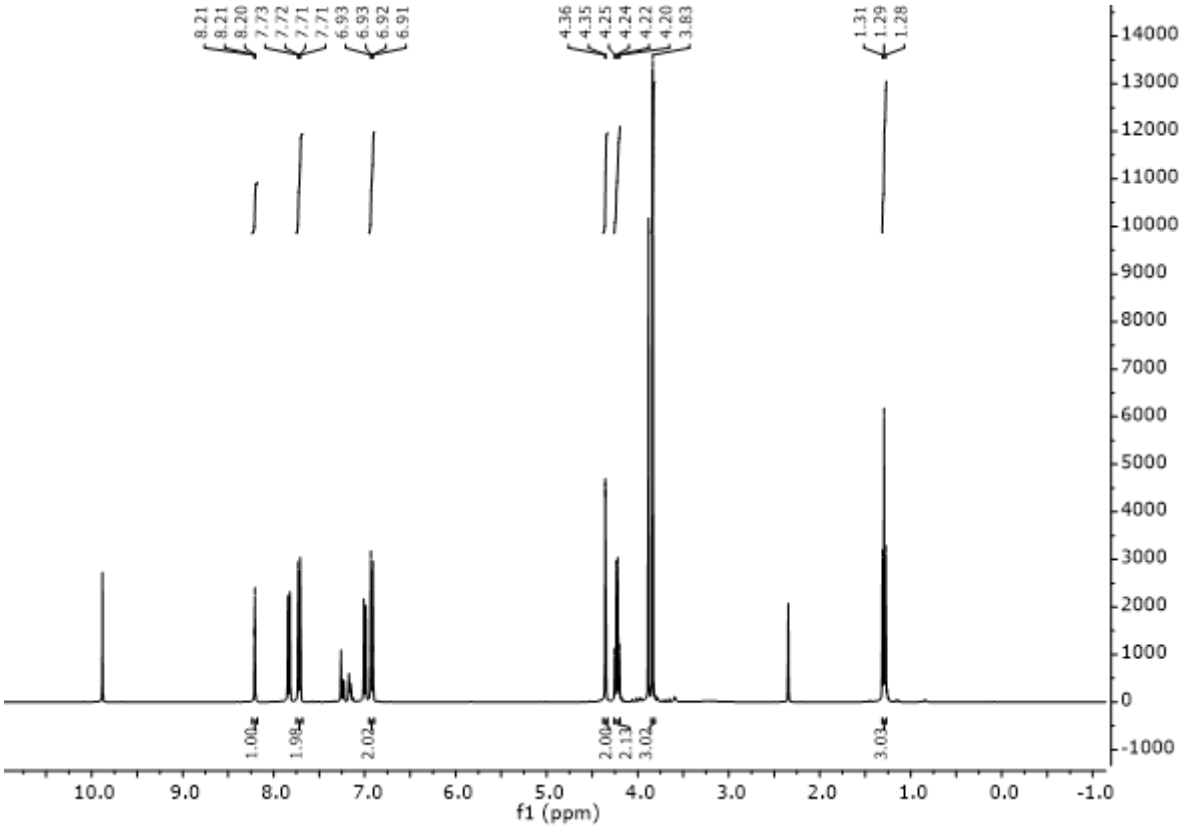

^{13}C-NMR

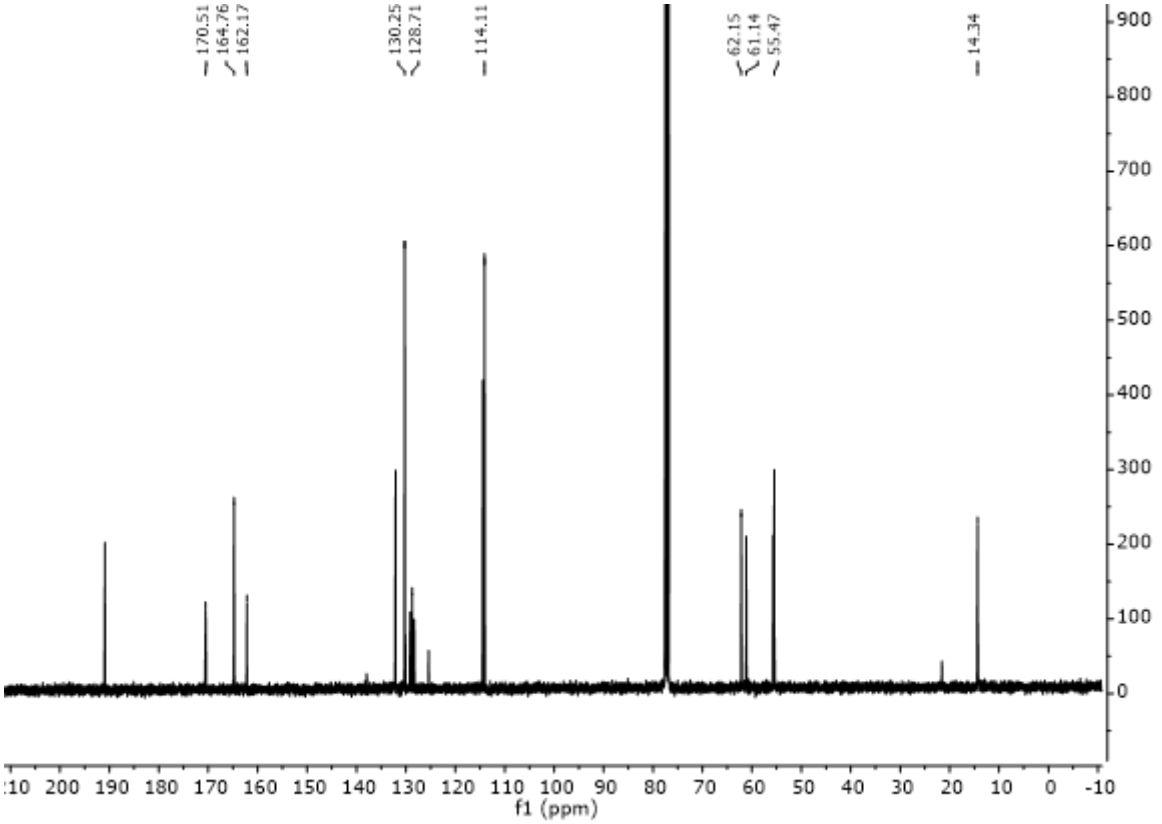

Ethyl 4-(methoxymethyl)-9*H*-pyrido[3,4-*b*]indole-3-carboxylate (**14**)

^{1}H-NMR

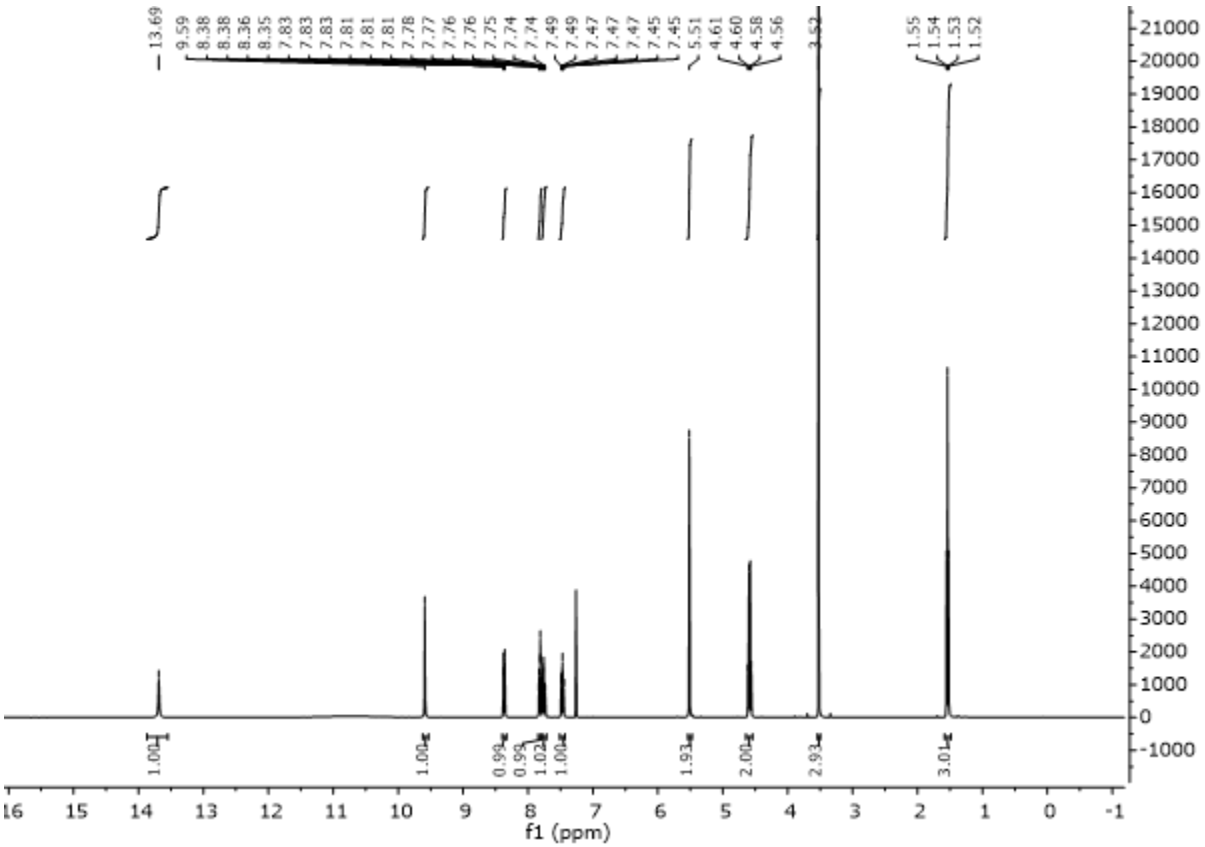

^{13}C-NMR

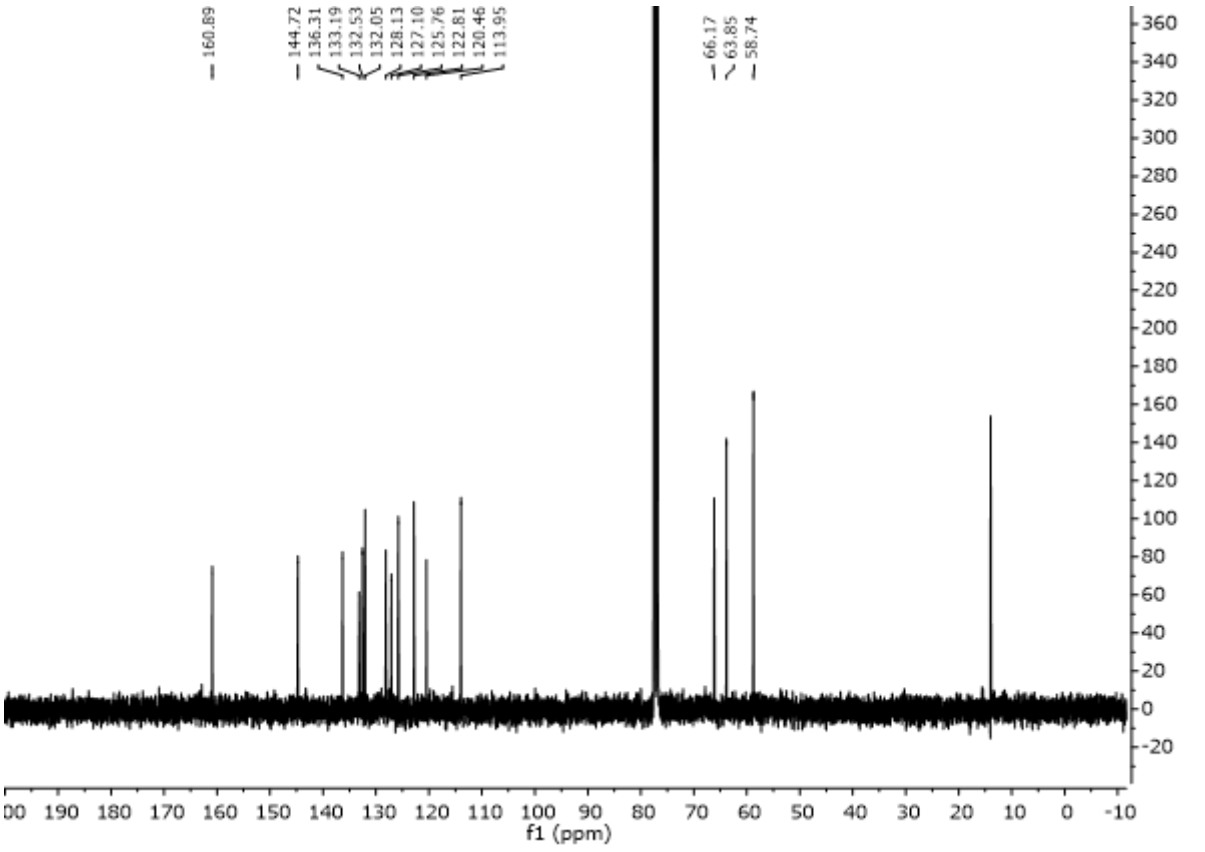

Ethyl 4-(methoxymethyl)-6-nitro-9*H*-pyrido[3,4-*b*]indole-3-carboxylate (**15**)

^{1}H-NMR

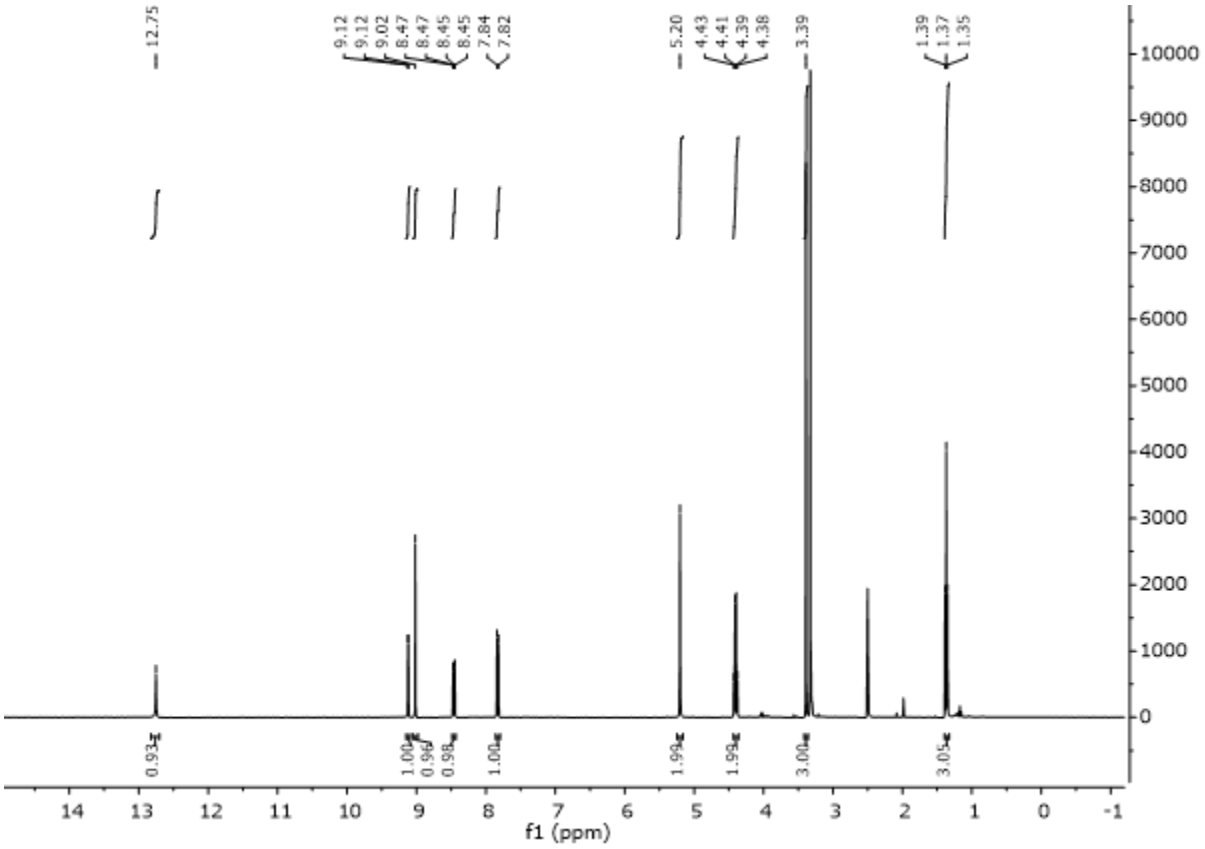

^{13}C-NMR

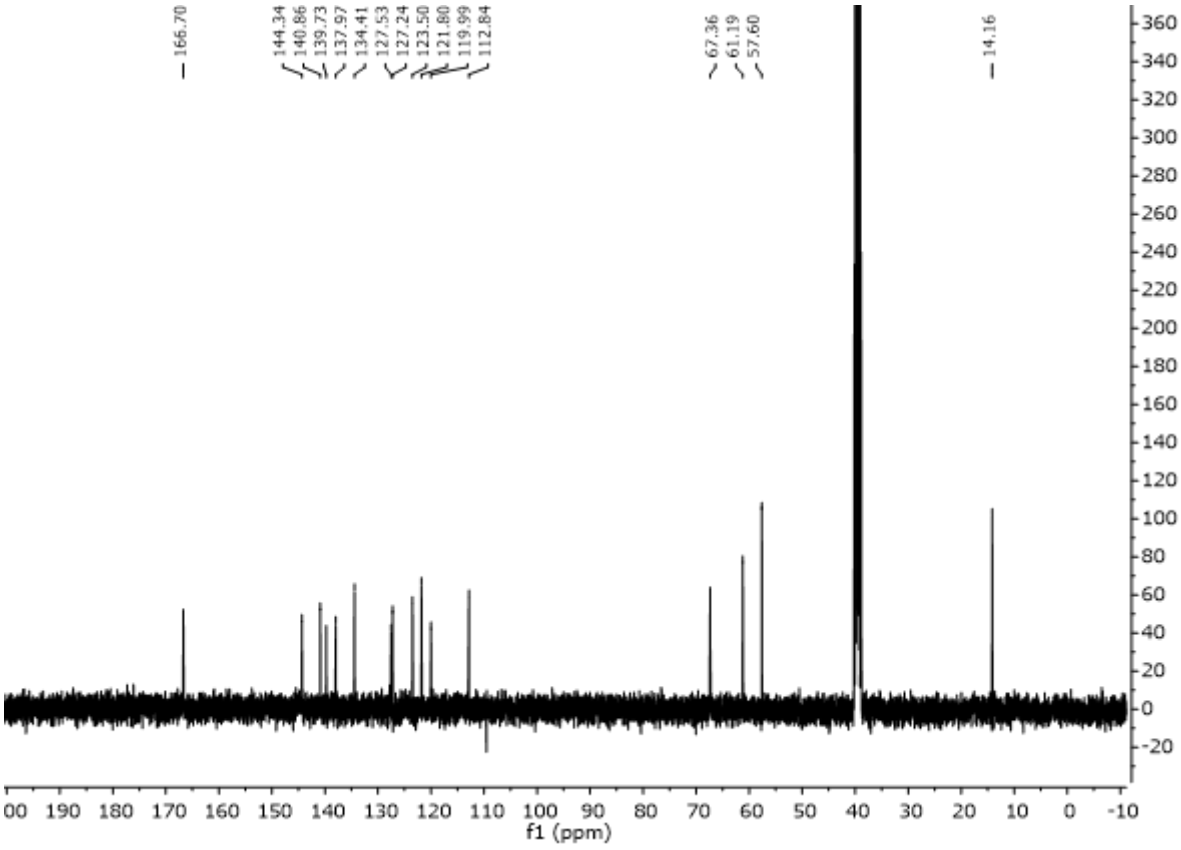

Ethyl 6-amino-4-(methoxymethyl)-9*H*-pyrido[3,4-*b*]indole-3-carboxylate (**16**)

^{1}H-NMR

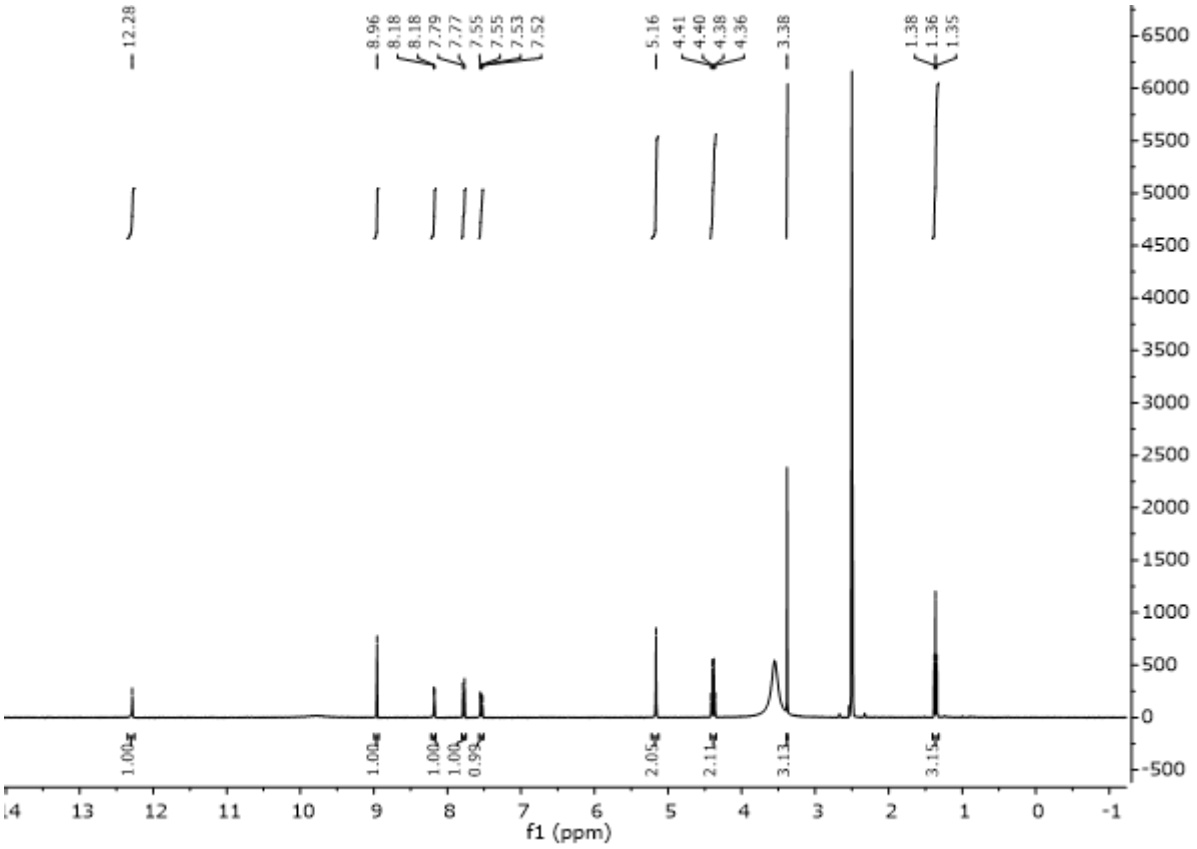

Ethyl (*E*)-4-(methoxymethyl)-6-(phenyldiazenyl)-9*H*-pyrido[3,4-*b*]indole-3-carboxylate (**1**)

^{1}H-NMR

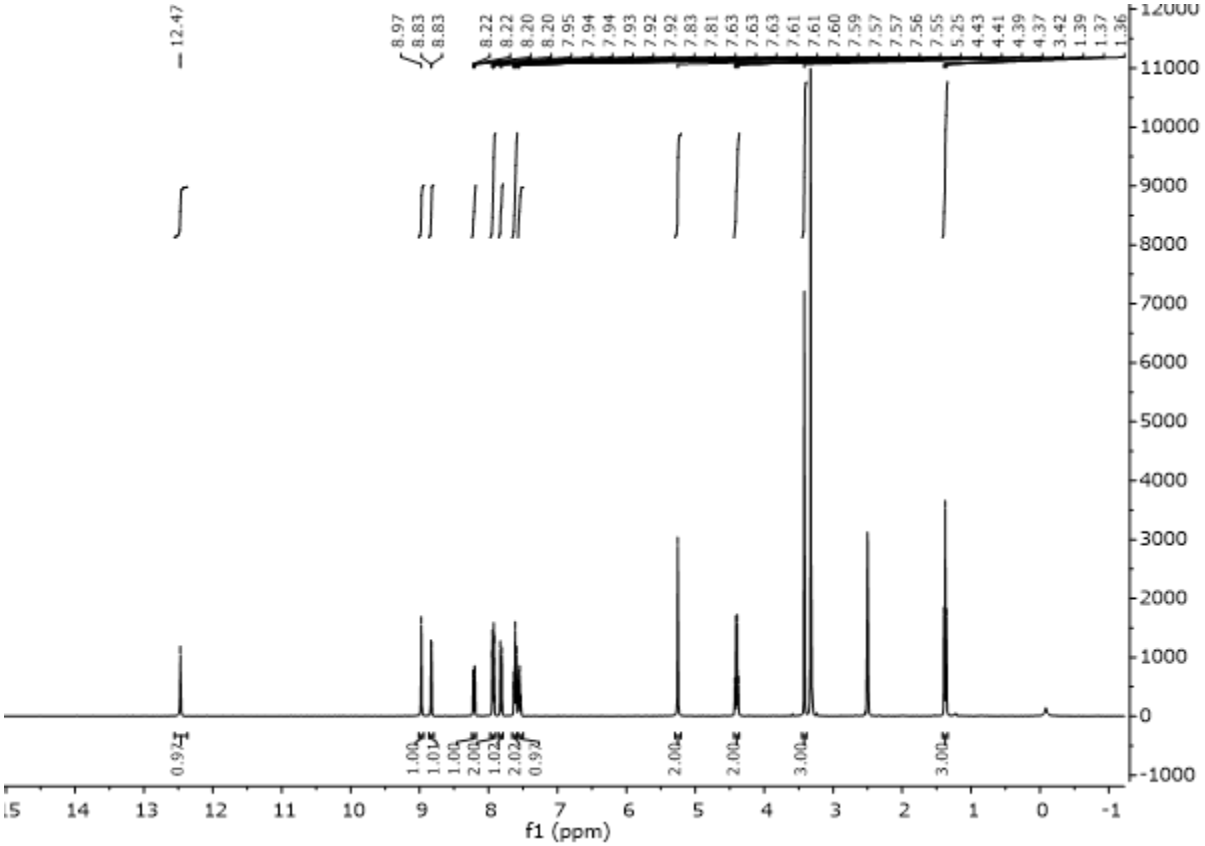

^{13}C-NMR

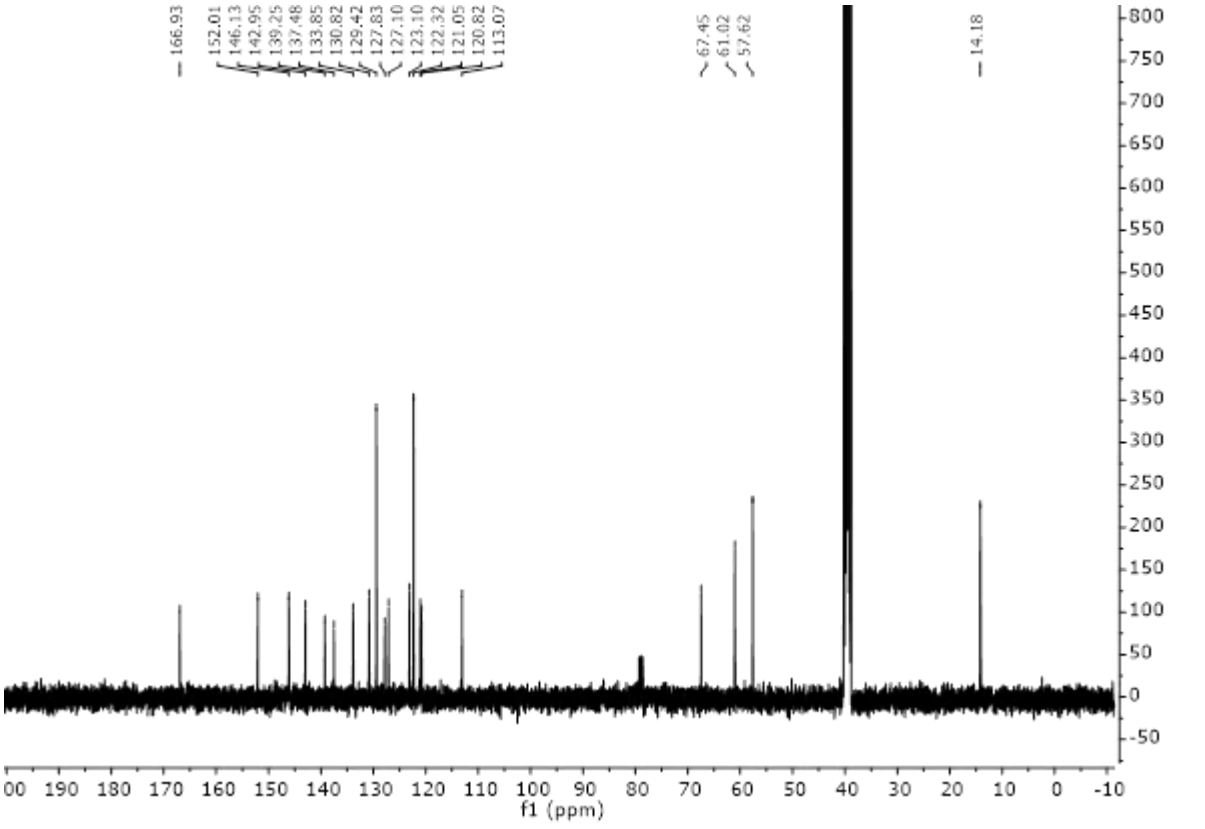

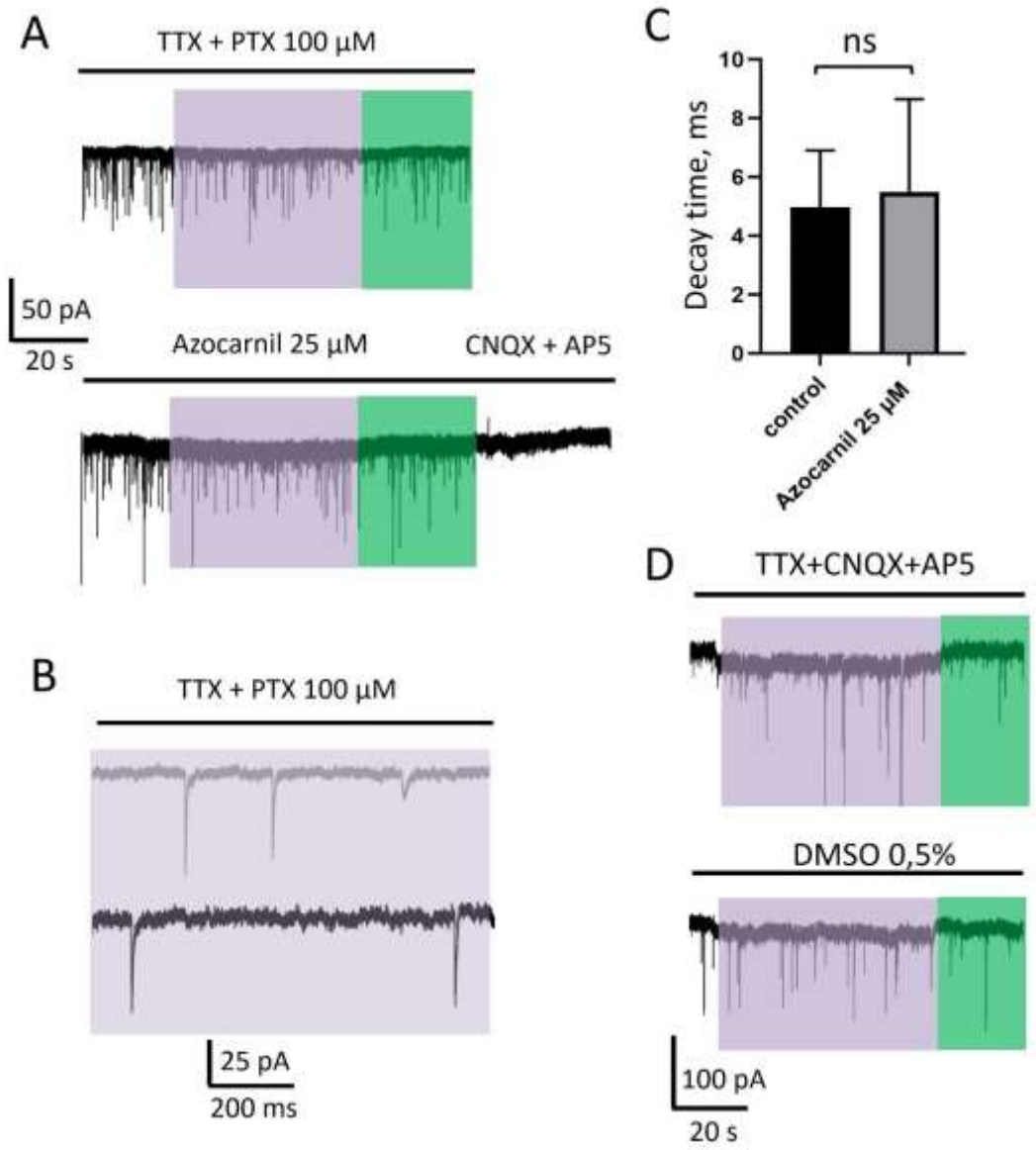

Figure S11. The effects of azocarnil on the glutamatergic currents and effect of the vehicle on GABAergic currents. (A) Voltage-clamp recordings of glutamatergic currents (represented in pA units, see scale bar at the bottom of the panel) in control conditions (during the application of TTX and PTX (100 µM)) and after addition of azocarnil (25 µM). Illumination with 400 nm and 500 nm light is indicated by violet and green rectangles respectively. A mixture of CNQX and AP5 was applied at the end of the recording to confirm the glutamatergic nature of recorded currents. **(B)** Magnified traces demonstrating single mEPSCs in control (gray trace) and during application of azocarnil (25 µM, black trace) during 400 nm illumination (violet rectangle). **(C)** Cumulative graph demonstrating the effect of azocarnil (25 µM) during 400 nm illumination on the decay time of mEPSCs. Comparison was done using unpaired t-test, n = 98 events from 3 independent experiments, ns – not significant. PTX: picrotoxin (GABA and Gly receptor pore blocker), TTX: tetrodotoxin, CNQX: 6-cyano-7-nitroquinoxaline-2,3-dione, AP5: (2R)-amino-5-phosphonovaleric acid. **(D)** Voltage-clamp recordings of GABAergic currents in control and after the addition of 0,5% of DMSO. Violet and green rectangles indicate illumination with 400 nm and 500 nm light, respectively.

Supplementary references

1. Trott, O. & Olson, A. J. AutoDock Vina: improving the speed and accuracy of docking with a new scoring function, efficient optimization, and multithreading. *J Comput Chem* **31**, 455–461 (2010).

2. Hanwell, M. D. *et al.* Avogadro: an advanced semantic chemical editor, visualization, and analysis platform. *J Cheminform* **4**, 1–17 (2012).
3. Frisch, M. gaussian 09, Revision d. 01, Gaussian. *Inc, Wallingford CT* **201**, (2009).
4. Kohn, W. & Sham, L. J. Quantum density oscillations in an inhomogeneous electron gas. *Physical Review* **137**, A1697 (1965).
5. Hohenberg, P. & Kohn, W. Inhomogeneous electron gas. *Physical review* **136**, B864 (1964).
6. Stephens, P. J., Devlin, F. J., Chabalowski, C. F. & Frisch, M. J. Ab initio calculation of vibrational absorption and circular dichroism spectra using density functional force fields. *J Phys Chem* **98**, 11623–11627 (1994).
7. Zhu, S. *et al.* Structural and dynamic mechanisms of GABAA receptor modulators with opposing activities. *Nat Commun* **13**, 4582 (2022).
8. Case, D. A. *et al. Amber 2021*. (University of California, San Francisco, 2021).
9. Durrant, J. D. & McCammon, J. A. BINANA: a novel algorithm for ligand-binding characterization. *J Mol Graph Model* **29**, 888–893 (2011).
10. Young, J., Garikipati, N. & Durrant, J. D. BINANA 2: characterizing receptor/ligand interactions in Python and JavaScript. *J Chem Inf Model* **62**, 753–760 (2022).
11. Kim, J. J. *et al.* Shared structural mechanisms of general anaesthetics and benzodiazepines. *Nature* **585**, 303–308 (2020).
12. Humphrey, W., Dalke, A. & Schulten, K. VMD: visual molecular dynamics. *J Mol Graph* **14**, 33–38 (1996).
13. Wehlan, H., Oehme, J., Schäfer, A. & Rossen, K. Development of Scalable Conditions for the Ugi Reaction Application to the Synthesis of (R)-Lacosamide. *Org Process Res Dev* **19**, 1980–1986 (2015).
14. Schwetlick, K. Organikum. (Wiley, 2009).
15. Rohlfs, G., & Vollert, B. (1995). Synthesis of 6-Benzyloxy-4-Methoxymethyl-[1,313 C2] β-Carboline-3-[13C] carboxylic Acid Isopropyl Ester (Abecarnil). Isotopes in Environmental and Health Studies, 31(3-4), 295-299.
16. Neef, G., Eder, U., Huth, A., Rahtz, D., Schmiechen R., Seidelmann D., *ChemInform* 14, (1983)
17. Ueno, K. & Akiyoshi, S. Kinetic study on the condensation reaction of aniline and nitrosobenzenes. J Am Chem Soc 76, 3670–3672 (1954).
18. Pagani, M. et al. How gastrin-releasing peptide opens the spinal gate for itch. *Neuron* **103**, 102–117 (2019).
19. Gonzalez-Cano, R. *et al.* Up–down reader: an open source program for efficiently processing 50% von Frey thresholds. *Front Pharmacol* **9**, 354777 (2018).
20. Kelly, M. D. *et al.* Role of the histidine residue at position 105 in the human α5 containing GABAA receptor on the affinity and efficacy of benzodiazepine site ligands. *Br J Pharmacol* **135**, 248–256 (2002).
21. Masiulis, S. *et al.* GABAA receptor signalling mechanisms revealed by structural pharmacology. *Nature* **565**, 454–459 (2019).
22. Crestani, F., Assandri, R., Täuber, M., Martin, J. R. & Rudolph, U. Contribution of the α1-GABAA receptor subtype to the pharmacological actions of benzodiazepine site inverse agonists. *Neuropharmacology* **43**, 679–684 (2002).
23. Kasaragod, V. B. *et al.* The molecular basis of drug selectivity for α5 subunit-containing GABAA receptors. *Nat Struct Mol Biol* **30**, 1936–1946 (2023).

24. Buhr, A., Baur, R. & Sigel, E. Subtle changes in residue 77 of the γ subunit of α1β2γ2 GABAA receptors drastically alter the affinity for ligands of the benzodiazepine binding site. *Journal of Biological Chemistry* **272**, 11799–11804 (1997).